NANO LETTERS

Letter

Scanning Tunnelling Spectroscopy on Arrays of CdSe Quantum Dots: Response of Wave Functions to Local Electric Fields

Lucian Jdira, Karin Overgaag, Jan Gerritsen, Danie#l Vanmaekelbergh, Peter Liljeroth, and Sylvia Speller

Nano Lett., **2008**, 8 (11), 4014-4019 • DOI: 10.1021/nl8026923 • Publication Date (Web): 10 October 2008

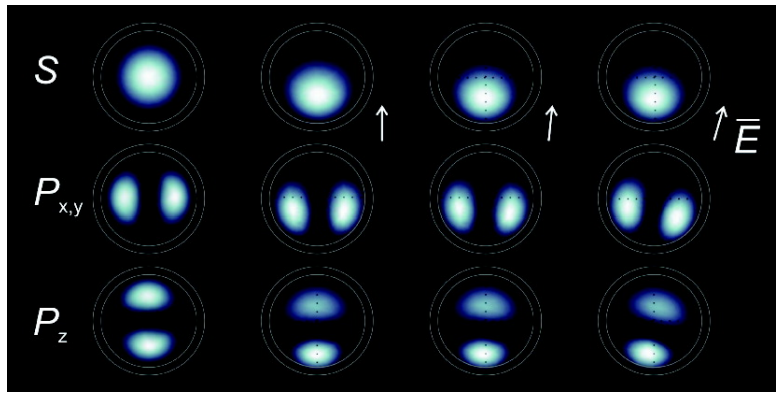

More About This Article

Additional resources and features associated with this article are available within the HTML version:

- Supporting Information
- Access to high resolution figures
- Links to articles and content related to this article
- Copyright permission to reproduce figures and/or text from this article

View the Full Text HTML

NANO LETTERS

2008
Vol. 8, No. 11
4014-4019

Scanning Tunnelling Spectroscopy on Arrays of CdSe Quantum Dots: Response of Wave Functions to Local Electric Fields

Lucian Jdira,[†,‡] Karin Overgaag,[†,§] Jan Gerritsen,[‡] Daniël Vanmaekelbergh,[§] Peter Liljeroth,[*,§] and Sylvia Speller[‡]

Institute for Molecules and Materials, Radboud University Nijmegen, PO Box 9010, 6500 GL Nijmegen, The Netherlands, Condensed Matter and Interfaces, Debye Institute for Nanomaterials Science, University of Utrecht, PO Box 80000, 3508 TA Utrecht, The Netherlands

Received September 4, 2008; Revised Manuscript Received September 26, 2008

ABSTRACT

We use scanning tunnelling microscopy (STM) to controllably contact individual CdSe quantum dots (QDs) in a multilayer array to study electrical contacts to a model QD solid. The probability of electron injection into the QD array depends strongly on the symmetry of the QD wave functions and their response to the local electric field. Quantitative spectroscopy of the QD energy levels is possible if the potential distribution in the STM tip−QD array−substrate system is taken into account.

Colloidal semiconductor nanocrystals are one the most actively studied components of modern nanoscience. The high degree of control over their size and shape makes it possible to accurately tune their optoelectronic properties through quantum confinement.[1−4] In the strong confinement regime, individual semiconductor QDs have widely spaced, discrete energy levels with atomlike envelope wave function symmetries (*S*, *P*, *D*, etc.). Semiconductor QDs can be used as building blocks for more complex architectures such as two- and three-dimensional superlattices.[2,5,6] This gives the opportunity to combine the quantum confinement in the individual QDs with the cooperative effects of a solid, with potential applications for novel optical and electronic devices.

With the size of the prospective devices shrinking rapidly, the drive to further miniaturize the active area to only a few QDs requires a rethinking of the electrical contacts.[7−12] The characteristics of the electrical contacts to the QD layer, i.e., the tunnelling contact between a macroscopic metal and a quantum system, are likely to be crucial in determining the device performance. The electric field due to the applied bias between the contacts gives rise to the (quantum confined) Stark effect, which will naturally affect the energies of the electronic levels.[13−17] In addition, the field will influence the spatial shape and extension of the wave functions in the nanocrystal host and thus the tunnelling contact. Depending on the direction of the field, it may also lift the degeneracy of the energy levels. The central questions are: (i) what is the role of the electric field distribution over the active device volume, and (ii) how does the symmetry of the quantum confined energy levels of the individual QDs affect the current transport in the device? These questions are equally relevant to the field of molecular devices.

In this paper, we use low-temperature scanning tunnelling microscopy (STM) and spectroscopy (STS) on multilayer arrays of colloidal CdSe QDs as a model system to controllably contact individual QDs in the first or second layer with the STM tip. The effects due to the field distribution can be probed locally and with high energy resolution. STS has been extensively used to measure the electronic spectrum of single, isolated semiconductor QDs, QD−metal heterostructures, and molecular QD aggregates.[18−25] In addition, studies of quantum mechanical coupling between QDs in self-assembled monolayers have been reported.[26,27] Prior to the present measurements, it was not clear whether a quantitative measurement of the local density of states (LDOS) is possible on arrays thicker than a monolayer: a QD bilayer already consists of an insulating film of >10 nm in thickness, seriously questioning the assumptions behind the simple field overtunnel barrier model that is commonly used in interpreting electron tunnelling

* Corresponding author. E-mail: p.liljeroth@uu.nl.
† These authors contributed equally to this work.
‡ Institute for Molecules and Materials, Radboud University Nijmegen.
§ Condensed Matter and Interfaces, Debye Institute for Nanomaterials Science, University of Utrecht.

10.1021/nl8026923 CCC: $40.75
Published on Web 10/10/2008

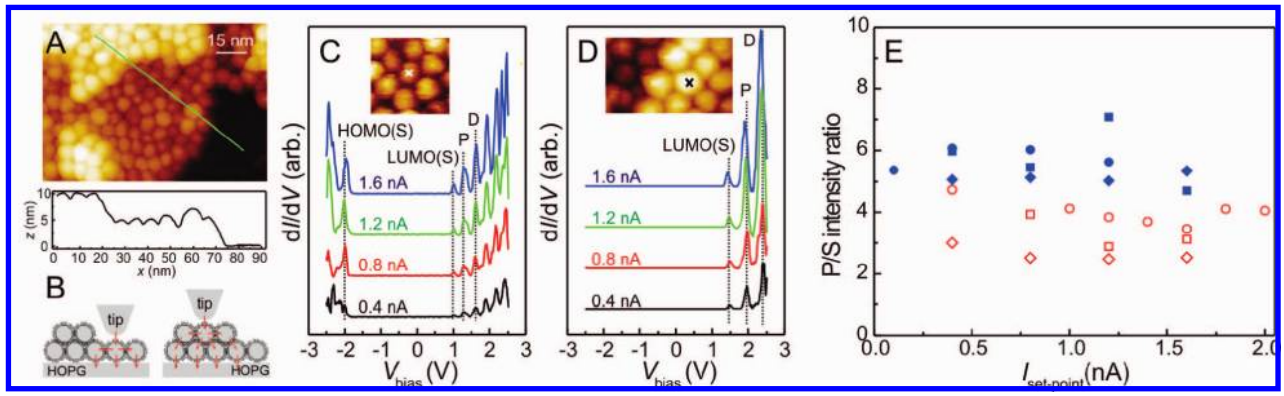

Figure 1. (A) STM topography of a bilayer of CdSe QDs (6.1 nm diameter) and a line profile. The measurement parameters are: tip−dot distance stabilized at 5 pA and 2.5 V. (B) Sketch of the relevant tunnelling processes in STS for QDs located in first and second layer, respectively. (C,D) Examples of d*I*/d*V* spectra measured in an array of CdSe QDs (6.1 nm diameter) in the first (C) and second (D) layer; the stabilization settings for spectroscopy were 0.4, 0.8, 1.2, and 1.6 nA at 2.5 V. Insets: STM topography of the investigated QDs. (E) The *P* to *S* peak intensity ratio as a function of set-point current for QDs located in first layer (empty symbols) or second layer (filled symbols).

spectroscopy.[28] We will show here that the QD energy levels can be measured quantitatively on both mono- and bilayers once the effect of the potential distribution over the tunnelling barriers and the QD layer has been taken into account. Furthermore, we establish "selection rules" for STS in a double-barrier tunnelling junction based on the spatial symmetries of the orbitals that are involved in the tunnelling processes. Finally, this understanding will be used to elucidate the effect of an asymmetric electric field on the electronic spectrum occurring at a step-edge of the QD layer.

CdSe QDs (diameter 6.1 nm with a size distribution <10%) were synthesized according to literature methods.[29,30] Hexagonal close-packed arrays were prepared by allowing a drop consisting of CdSe QDs dissolved in $CHCl_3$ solution to slowly dry on an atomically flat HOPG substrate. A second drop-cast allows the QDs to self-organize into a bilayer QD structure. The interdot distance is determined by the organic ligands (trioctylphosphine oxide, TOPO) that terminate the QD surface. The samples were heated up to 150 °C in ultrahigh vacuum (UHV) overnight prior to the STM experiments. Vacuum annealing leads to interdigitation and possibly, evaporation, of the capping molecules as evidenced by the stability of the QD arrays under STM imaging and small interparticle separation.[31] Thermal decomposition of the capping molecules at these temperatures is very unlikely.[32] All STM experiments were carried out at 4.8 K with an UHV STM (LT STM, Omicron Nanotechnology). STM images were taken in the constant-current mode using W or PtIr tips (typically bias of 2−2.5 V and set-point current of 5−20 pA). The tunnelling spectra were acquired by choosing a QD of interest in the array and stabilizing the STM tip above its center. We performed STS at different locations within the assembly, on QDs in the first and second layer, in the middle of the array and at the step-edges.

A topographic image of a bilayer structure of CdSe QDs (6.1 nm diameter) is shown in Figure 1a. The layers show local hexagonal packing, but lack true long-range order due to size and shape distribution of the nanocrystal building blocks. The line profile gives an average center-to-center spacing of ∼7 nm and hence, ∼1 nm spacing between the QDs. We note that this interdot spacing is consistent with the QD separation measured using small-angle X-ray scattering on close-packed CdSe QD arrays capped with the same capping molecules.[33] To examine the electronic structure, we can select any QD of interest for tunnelling spectroscopy. Figure 1b shows the relevant tunnelling processes in STS experiments involving QDs located in the first and second layer. The current response is mainly determined by the following factors: the tunnelling rates into (Γ_{in}) and out (total rate Γ_{out}) of the QD under investigation, the bias voltage distribution over the tunnelling junctions and the QD layer, and the interdot quantum mechanical coupling (covalent interactions). If Γ_{in} is smaller than Γ_{out} (shell-tunnelling spectroscopy), the electrons tunnel one-by-one through the QD and charging effects are absent.[20,34,35] The bias distribution over the tunnelling junctions and the QD layer influences the measured zero-conductivity gap and the separations between the resonances in the tunnelling spectra.[34,35] This effect has to be taken into account in converting the measured d*I*/d*V* spectra from the bias scale to the true energy scale. Strong quantum mechanical coupling between QD wave functions in arrays affects the widths of the tunnelling resonances, which leads to broadened features in tunnelling spectra.[26,27] On the other hand, if the coupling is weak and the electron (hole) states are not delocalized over neighboring QDs, we should observe tunnelling resonances with widths equal to those of individual QDs.

Examples of the tunnelling spectra measured in the first layer are shown in Figure 1c (further examples to illustrate the reproducibility of the results are given in the Supporting Information). The spectra exhibit a zero-conductance gap (difference between the highest occupied molecular orbital (HOMO) and the lowest unoccupied molecular orbital (LUMO)) with resonances at negative and positive bias corresponding to the valence (hole) and conduction (electron) levels, respectively. Increasing the set-point current from 0.4 to 1.6 nA has no effect on the bias position of the resonances, only the intensity of the peaks is increased by decreasing

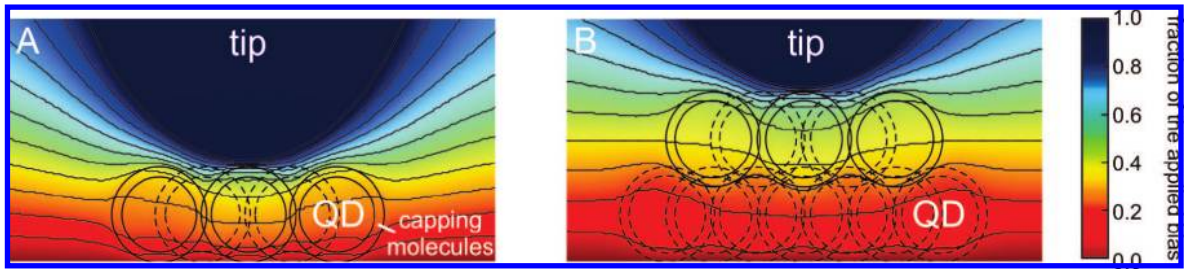

Figure 2. Potential distribution in the tip−QD substrate junction obtained by solving the Laplace equation in a realistic geometry with 6 nm diameter QDs, organic ligands with a length of 0.5 nm, and a typical tip−QD separation of 1.0 nm: a monolayer (A) and bilayer (B) of CdSe QDs. The dielectric constants used in the calculations are: 10 for CdSe and 3 for the capping molecules.

tip−QD separation (increasing set-point current), confirming shell-tunnelling conditions.[20,34] Figure 1d shows tunnelling spectra measured on a dot located in the second layer (the dot is indicated in the inset). Resonances are only observed at positive bias, corresponding to tunnelling through conduction levels. In an attempt to access the valence hole levels, we found that at biases exceeding −2.5 V, the tunnelling conditions become unstable. In the following, we only consider electron injection from the STM tip into the QD conduction levels. As for the tunnelling spectra on QDs in the first layer, the spectral features were independent of the tip−QD distance, confirming shell-tunnelling conditions. This implies that we measure the single-electron energy levels and hence, electron−electron repulsion is absent. The tunnelling spectra measured on CdSe QDs in the first and second layer exhibit the signature of zero-dimensional density of states, with peaks widths comparable to isolated CdSe QDs.[31] This indicates weak quantum mechanical coupling between QDs in the mono- and multilayer arrays. Thus, we ascribe the resonances in the d*I*/d*V* spectra to quantum confined energy levels with atomlike envelope wave function symmetries: *S* (LUMO), *P*, *D*, etc. The absence of quantum mechanical coupling is consistent with earlier results based on transport measurements, charge imaging, and optical experiments.[36−39]

The spectra recorded on QDs in the second layer show resonances located at higher bias than on QDs in the first layer. To understand this, we have to consider the bias voltage distribution between the STM tip and the substrate. In STS experiments, the applied bias between tip and substrate does not drop completely across the tip−QD junction, thus the bias voltage at a resonance in the tunnelling spectrum is related to the QD energy levels (E_i) through: $\eta V_{\text{bias}} = E_i + \Sigma_i$, where Σ_i is the polarization energy and η corresponds to the ratio between the potential drop in the tip−QD junction and the applied bias.[35] As a result, the measured zero-conductivity gap is always larger than the quasiparticle gap by a factor $1/\eta$. We estimate η by solving the Laplace equation numerically (COMSOL Multiphysics 3.4, Comsol Ab, Sweden) for a realistic tip−QD−substrate geometry (with tip radius of 10 nm and tip-to-dot distance of 1 nm) with 6 nm diameter QDs and dielectric constants of 10 for CdSe and 3 for organic molecules. The results are shown in Figure 2a,b. Depending on the exact shape of the tip and the tip-to-dot and dot-to-substrate distances, we find that η is on average 0.70 ± 0.05 and 0.55 ± 0.05 for a QD in the middle of the first or second layer, respectively. Multiplying the measured *S*-to-*P* peak separation by this factor yields an energy difference between the *S*- and the *P*-levels of 0.22 ± 0.02 and 0.26 ± 0.02 eV for QDs in the first and second layer, respectively. Tight-binding calculations predict an *S*−*P* energy separation of 0.230 eV for QDs of this size.[15] These results show that it is possible to obtain quantitative information on the energy level positions of individual QDs in QD multilayers provided that an independent estimate of the bias distribution over the entire system is available. This is an important result for future experiments on three-dimensional binary QD superlattices.

We plot the intensity ratio of the *P* to *S* resonances for shell-tunnelling spectra measured on several QDs in the first and second layer in Figure 1e. Interestingly, the ratio measured on CdSe QDs located in the first and second layer differs by almost a factor of 2. In the shell-tunnelling regime, the total current is limited by tunnelling from the tip into the QD. Hence, the tunnelling current is $I = e\Sigma_i\Gamma_{\text{in},i}$, where $\Gamma_{\text{in},i}$ is the tunnelling rate from the tip to the level i in the QD. Consequently, it might be expected that the *P* to *S* peak intensity ratio is proportional to the degeneracy of the energy levels, i.e., an amplitude ratio of 3 for QDs either in the first or second layer. However, experimental evidence does not confirm these expectations. We found the *P*-to-*S* peak intensity ratio to be on average 3.4 ± 0.7 for spectra measured on QDs in the first layer and 5.6 ± 0.6 for spectra measured on QDs in the second layer. In addition, the *P*-to-*S* peak intensity ratio does not depend on the tip−QD distance in the investigated set-point current range (Figure 1e). To understand the failure of intuitive reasoning, the symmetry of the *P* orbitals and the effect of the electric field have to be taken into account.

In STS experiments, because of the applied bias over the tip−QD−substrate junction, the QD is exposed to a considerable electric field. It is well-known based on theory and experiment that both the energies and the distribution of electron densities of the QD eigenstates are affected due to the quantum confined Stark effect (QCSE).[4,13,14,16,17,35,40,41] Consequently, the electric field can influence the tip−QD wave function overlap, resulting in different current intensities for orbitals with different symmetries. We estimate these effects by solving the Schrödinger equation for CdSe QDs in an electric field based on the solution of the Laplace equation in a realistic tip−QD−substrate configuration. The particle-in-a-sphere eigenfunctions in the absence of an

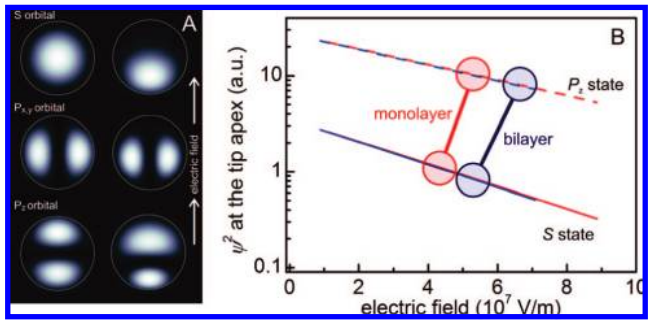

Figure 3. Solution of the Schrödinger equation in the electric field set up in the STM tip−substrate junction. (A) Plots of the squares of the wave functions with S, $P_{x,y}$, and P_z envelope symmetry in the absence (left) and presence of an electric field (right). (B) ψ^2 at the tip apex for the S (solid lines) and P_z (dashed lines) states on a QD in a monolayer (red) and a bilayer (blue) as a function of the average electric field in the QD. The circles indicate the electric fields corresponding to the bias voltages of the S and P resonances in the experiment for the monolayer (red) and bilayer (blue), respectively.

electric field are plotted in Figure 3a (left). The first eigenvalue corresponds to the envelope wave function having S type symmetry ($n = 1$, $l = 0$). The first exited state has P type symmetry ($n = 1$, $l = 1$) and is 3-fold degenerate (P_x, P_y, and P_z with $m = 0, \pm 1$). Resonant tunnelling from the tip into the QD depends on the overlap between the tip and QD wave functions;[28] if the tip is positioned directly above the center of the QD, tunnelling through P_x and P_y levels has a very low probability (nodal plane). Hence, in the absence of a lateral electric field (vide infra), only the P_z state contributes to the tunnelling current. We will next consider in detail how the S and P_z states respond to the electric field in the STM−substrate junction and how this depends on whether we carry out the measurement on the first or second QD layer.

The response of wave functions with S, $P_{x,y}$, and P_z envelope symmetry to the electric field under the STM tip is shown in Figure 3a (right). In the calculation, we neglect quantum mechanical coupling between the QDs, i.e., we only consider the QD directly under the tip in the solution of the Schrödinger equation. As a result of the potential distribution in the STM tip−substrate junction, the wave functions respond to the electric field by shifting along the field direction, Figure 3a (right). Two consequences emerge from this effect. First, energy is gained by redistributing the electron density in the electric field, i.e., Stark shift. For 6 nm diameter CdSe QDs, the calculated Stark shift is roughly 10 meV for the S state. Observing this shift quantitatively in our experiment is not possible due to the QD size and shape distribution. The second consequence is that it makes the overlap between the QD and tip wave functions smaller and hence affects the resonant tunnelling probability, i.e., the amplitude of the dI/dV signal in the experiment.

In the Tersoff−Hamann formalism,[28] the tunnelling current (and hence the dI/dV signal) is proportional to the square of the wave function of a given state at the position of the STM tip and thus depends on how the QD wave functions extend outside the nanocrystal. As a result of the electric field, the electron density shifts away from the tip and the ψ^2 at the tip apex is reduced with increasing bias (Figure 3b). According to our calculations, the ψ^2 at the tip apex for the S and P_z states is only a function of the electric field in the QD and does not depend on whether the dot is in the first or second layer of the array. In addition, at a given bias, the average electric field in the QD directly under the STM tip is roughly equal for a QD in the first and the second layer. However, because of the voltage distribution in the STM junction, the bias voltage at resonance and hence the electric field is larger on a bilayer compared to a monolayer (red and blue circles in Figure 3b). Theoretically, we find roughly a 20% increase in the P_z to S intensity ratio, confirming that the difference in the measured tunnelling spectra for CdSe is not an intrinsic effect but simply the change in the electric field distribution going from the first to the second layer. The fair correspondence between theory and experiment also supports our idea that only one of the P orbitals (P_z) is involved in electron tunnelling. To quantitatively relate the measured intensity of the resonances in the dI/dV spectra to the true LDOS, it is necessary to consider in detail the spatial extension of the wave functions involved in the tunnelling processes.

Figure 4 presents correlated topography-spectroscopy results acquired on QDs at different locations of the bilayer structure. The investigated QDs are labeled in Figure 4a. The spectrum measured on QDs in the first layer (QD1) shows resonances at both positive and negative bias (Figure 4b) in agreement with the measurements shown in Figure 1c. Similarly to the results shown in Figure 1d, the spectra of QDs located in the middle of the array in the second layer (QD2 and QD3) show three peaks at positive bias corresponding to the tunnelling through S, P_z, and D states in the shell-tunnelling regime (Figure 4c). Surprisingly, the spectra measured on QDs at the periphery of the second layer (QD4 and QD5) show an additional peak, as illustrated in Figure 4d. Which tunnelling processes are responsible for this additional resonance? Varying the set-point current between 0.1 and 0.8 nA shows that these spectra are also measured under shell-tunnelling, i.e., the additional resonance is not related to a lifting of the level degeneracy by Coulomb interactions. A possible hypothesis is that the two closely spaced resonances correspond to tunnelling through the different P levels. However, the QCSE alone is not sufficient to explain the experimental energy separation (after correcting for the bias distribution) of ca. 100 meV between the two peaks at a bias of ca. 2 V in Figure 4d. There has to be another physical reason for the magnitude of the observed splitting of the P levels. It is well-known that the typical synthesis conditions yield CdSe QDs that are slightly prolate due to the wurtzite crystal structure of CdSe. The long axis of the QD corresponds to the c-axis of the crystal (typical aspect ratio of ca. 1.2), and it is oriented parallel to the substrate.[2,42] On the basis of effective mass calculations, the expected energy splitting between the P levels due to the nonspherical shape of the QD is indeed on the order of 100 meV, in good agreement with the peak separation in the tunnelling spectra in Figure 4d. It is thus

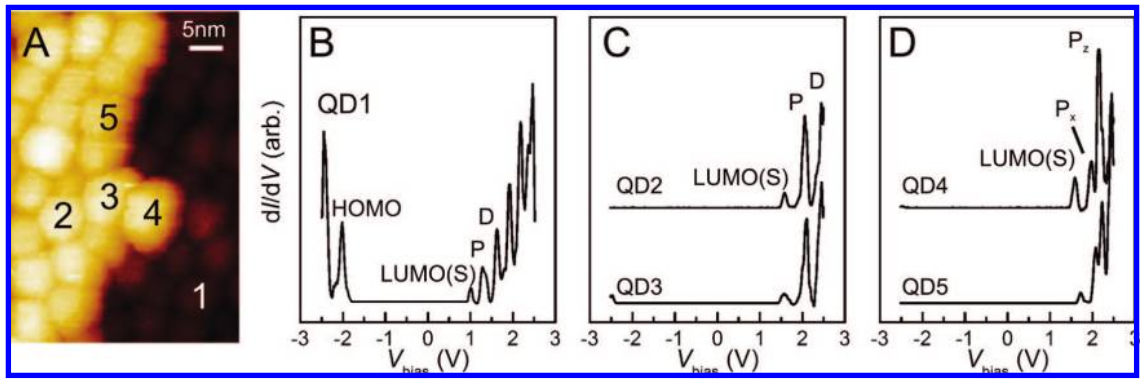

Figure 4. Dependence of the spectroscopic response on the location of the QDs in the assembly. (A) Topographic image of the 6.1 nm CdSe QDs at a set-point current 5 pA and a bias 2.5 V. Examples of d*I*/d*V* spectra measured on (B) a QD in the first layer, (C) QDs in the second layer, and (D) QDs at the periphery of the second layer.

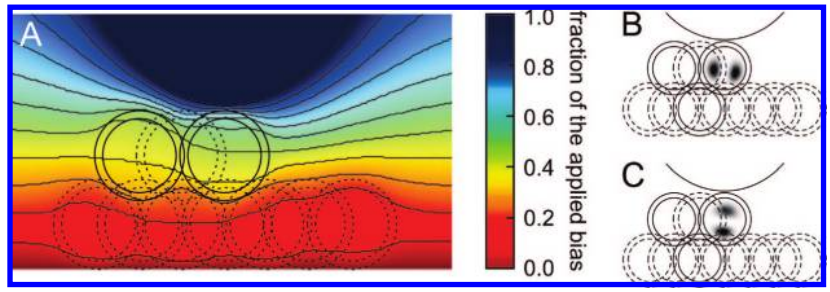

Figure 5. (A) Calculation of the electric potential distribution when the STM tip is positioned on a QD at the periphery of the second layer. Response of the wave functions to this potential distribution for the P_x (B) and P_z (C) orbitals.

reasonable to assign the two peaks in the spectra in Figure 4d to tunnelling through P_x (parallel to the *c*-axis, lower bias) and P_z states (perpendicular to the *c*-axis, higher bias). The remaining challenge is to explain how tunnelling through the P_x level (oriented along the *c*-axis of the QD crystal, i.e., parallel to the substrate) has a much higher probability for a QD at the periphery compared to one in the interior of the array.

In Figure 5a, we show the calculated potential distribution for a QD at the periphery of the second layer. Because of the asymmetry of the geometry at the periphery of the layer, there is a lateral component of the electric field within the QD directly under the STM tip. This asymmetric field deforms the QD wave functions; the calculated ψ^2 for the P_x and P_z orbitals is shown in Figure 5b,c, respectively. In particular, the orientation of the P_x orbital is rotated with respect to the *xy*-plane. This reorientation of the wave function makes it possible to have tunnelling through this orbital even though the STM tip is located over the center of the QD, resulting in an additional peak in tunnelling spectra. While the calculations predict orders of magnitude increase in the tunnelling probability through the P_x level due to the lateral electric field, the experimental magnitude of the P_x resonance is not fully reproduced. The remaining discrepancy might be due to, for example, the presence of a permanent crystal dipole. The lateral electric field is absent for QDs located well in the array and, consequently, the STM tip above the center of the QD is at the nodal plane of the P_x and P_y wave functions.

In conclusion, we have demonstrated how STM and STS can be used to controllably contact and probe QDs in multilayer assemblies. Quantitative spectroscopy of the QD energy levels is possible if the potential distribution in the STM tip−substrate junction is properly taken into account. The probability of electron injection into the QD assembly depends strongly on the symmetry of the QD wave functions and their response to the local electric field set up by the contacts. In particular, the presence of an asymmetric electric field at the step-edge of the QD array can break the symmetry of the wave functions and open tunnelling channels that otherwise have zero probability of transmission. Our results are important for understanding how the electrical contacts between a macroscopic metal and a QD solid work. We show that an electric field can affect the carrier wave functions in QDs in several ways and hence, influence the performance of opto-electronic devices based on QD solids.[8,43,44] Future devices will require control of the tunnel contacts in terms of energy and wave function symmetry and should not overlook local irregularities in the QD array.

Acknowledgment. This work was supported by The Netherlands Foundation for Fundamental Research on Matter (FOM), Nederlandse Organisatie voor Wetenschappelijk Onderzoek (NWO/Chemical Sciences, Vidi-grant 700.56.423, P.L.), NanoNed, the Dutch nanotechnology program of the Ministry of Economic Affairs, and by the European projects "Advanced Scanning Probes for Innovative Nanoscience and Technology". We gratefully acknowledge Arjan Houtepen and Celso de Mello Donegá for the nanocrystal samples used in this study.

Supporting Information Available: Further examples of the tunnelling spectra measured on the QDs in the first and

second layer. This material is available free of charge via the Internet at http://pubs.acs.org.

References

(1) Alivisatos, A. P. *J. Phys. Chem.* **1996**, *100*, 13226–13239.
(2) Murray, C. B.; Kagan, C. R.; Bawendi, M. G. *Annu. Rev. Mater. Sci.* **2000**, *30*, 545–610.
(3) Manna, L.; Scher, E. C.; Alivisatos, A. P. *J. Am. Chem. Soc.* **2000**, *122*, 12700–12706.
(4) Muller, J.; Lupton, J. M.; Lagoudakis, P. G.; Schindler, F.; Koeppe, R.; Rogach, A. L.; Feldmann, J.; Talapin, D. V.; Weller, H. *Nano. Lett.* **2005**, *5*, 2044–2049.
(5) Redl, F. X.; Cho, K. S.; Murray, C. B.; O'Brien, S. *Nature* **2003**, *423*, 968–971.
(6) Chen, Z.; O'Brien, S. *ACS Nano* **2008**, *2*, 1219–1229.
(7) Klein, D. L.; Roth, R.; Lim, A. K. L.; Alivisatos, A. P.; McEuen, P. L. *Nature* **1997**, *389*, 699–701.
(8) Talapin, D. V.; Murray, C. B. *Science* **2005**, *310*, 86–89.
(9) Hu, Z. H.; Fischbein, M. D.; Querner, C.; Drndic, M. *Nano Lett.* **2006**, *6*, 2585–2591.
(10) Black, C. T.; Murray, C. B.; Sandstrom, R. L.; Sun, S. H. *Science* **2000**, *290*, 1131–1134.
(11) Parthasarathy, R.; Lin, X. M.; Jaeger, H. M. *Phys. Rev. Lett.* **2001**, *8718*, 186807.
(12) Beecher, P.; Quinn, A. J.; Shevchenko, E. V.; Weller, H.; Redmond, G. *Nano Lett.* **2004**, *4*, 1289–1293.
(13) Empedocles, S. A.; Bawendi, M. G. *Science* **1997**, *278*, 2114–2117.
(14) Tews, M.; Pfannkuche, D. *Phys. Rev. B* **2002**, *65*, 073307.
(15) Delerue, C.; Lannoo, M., *Nanostructures; Theory and Modelling*; Springer: Berlin, 2004.
(16) Wen, G. W.; Lin, J. Y.; Jiang, H. X.; Chen, Z. *Phys. Rev. B* **1995**, *52*, 5913.
(17) Li, S.-S.; Xia, J.-B. *J. Appl. Phys.* **2000**, *88*, 7171–7174.
(18) Banin, U.; Cao, Y. W.; Katz, D.; Millo, O. *Nature* **1999**, *400*, 542–544.
(19) Banin, U.; Millo, O. *Annu. Rev. Phys. Chem.* **2003**, *54*, 465–492.
(20) Bakkers, E. P. A. M.; Hens, Z.; Zunger, A.; Franceschetti, A.; Kouwenhoven, L. P.; Gurevich, L.; Vanmaekelbergh, D. *Nano. Lett.* **2001**, *1*, 551–556.
(21) Liljeroth, P.; Zeijlmans van Emmichoven, P. A.; Hickey, S. G.; Weller, H.; Grandidier, B.; Allan, G.; Vanmaekelbergh, D. *Phys. Rev. Lett.* **2005**, *95*, 086801.
(22) Steiner, D.; Mokari, T.; Banin, U.; Millo, O. *Phys. Rev. Lett.* **2005**, *95*, 056805.
(23) Overgaag, K.; Liljeroth, P.; Grandidier, B.; Vanmaekelbergh, D. *ACS Nano* **2008**, *2*, 600–606.
(24) Katz, D.; Wizansky, T.; Millo, O.; Rothenberg, E.; Mokari, T.; Banin, U. *Phys. Rev. Lett.* **2002**, 89.
(25) Bernard, R.; Comtet, G.; Dujardin, G.; Huc, V.; Mayne, A. J. *Appl. Phys. Lett.* **2005**, *87*, 053114.
(26) Liljeroth, P.; Overgaag, K.; Urbieta, A.; Grandidier, B.; Hickey, S. G.; Vanmaekelbergh, D. *Phys. Rev. Lett.* **2006**, *97*, 096803.
(27) Steiner, D.; Aharoni, A.; Banin, U.; Millo, O. *Nano. Lett.* **2006**, *6*, 2201–2205.
(28) Tersoff, J.; Hamann, D. R. *Phys. Rev. B* **1985**, *31*, 805.
(29) Murray, C. B.; Norris, D. J.; Bawendi, M. G. *J. Am. Chem. Soc.* **1993**, *115*, 8706–8715.
(30) de Mello Donegá, C.; Hickey, S. G.; Wuister, S. F.; Vanmaekelbergh, D.; Meijerink, A. *J. Phys. Chem. B* **2003**, *107*, 489–496.
(31) Jdira, L.; Overgaag, K.; Stiufiuc, R.; Grandidier, B.; Delerue, C.; Speller, S.; Vanmaekelbergh, D. *Phys. Rev. B* **2008**, *77*, 205308.
(32) Perez-Dieste, V.; Castellini, O. M.; Crain, J. N.; Eriksson, M. A.; Kirakosian, A.; Lin, J. L.; McChesney, J. L.; Himpsel, F. J.; Black, C. T.; Murray, C. B. *Appl. Phys. Lett.* **2003**, *83*, 5053–5055.
(33) Kagan, C. R.; Murray, C. B.; Nirmal, M.; Bawendi, M. G. *Phys. Rev. Lett.* **1996**, *76*, 1517–1520.
(34) Jdira, L.; Liljeroth, P.; Stoffels, E.; Vanmaekelbergh, D.; Speller, S. *Phys. Rev. B* **2006**, *73*, 115305.
(35) Niquet, Y. M.; Delerue, C.; Allan, G.; Lannoo, M. *Phys. Rev. B* **2002**, *65*, 165334.
(36) Yu, D.; Wang, C. J.; Guyot-Sionnest, P. *Science* **2003**, *300*, 1277–1280.
(37) Drndic, M.; Markov, R.; Jarosz, M. V.; Bawendi, M. G.; Kastner, M. A.; Markovic, N.; Tinkham, M. *Appl. Phys. Lett.* **2003**, *83*, 4008–4010.
(38) Drndic, M.; Jarosz, M. V.; Morgan, N. Y.; Kastner, M. A.; Bawendi, M. G. *J. Appl. Phys.* **2002**, *92*, 7498–7503.
(39) Kim, B. S.; Islam, M. A.; Brus, L. E.; Herman, I. P. *J. Appl. Phys.* **2001**, *89*, 8127–8140.
(40) Mendez, E. E.; Bastard, G.; Chang, L. L.; Esaki, L.; Morkoc, H.; Fischer, R. *Phys. Rev. B* **1982**, *26*, 7101.
(41) Kraus, R. M.; Lagoudakis, P. G.; Rogach, A. L.; Talapin, D. V.; Weller, H.; Lupton, J. M.; Feldmann, J. *Phys. Rev. Lett.* **2007**, *98*, 017401.
(42) Murray, C. B.; Kagan, C. R.; Bawendi, M. G. *Science* **1995**, *270*, 1335–1338.
(43) Coe, S.; Woo, W. K.; Bawendi, M.; Bulovic, V. *Nature* **2002**, *420*, 800–803.
(44) Konstantatos, G.; Howard, I.; Fischer, A.; Hoogland, S.; Clifford, J.; Klem, E.; Levina, L.; Sargent, E. H. *Nature* **2006**, *442*, 180–183.

NL8026923